Chinese Journal of
POLYMER SCIENCE

FEATURE ARTICLE

https://doi.org/10.1007/s10118-018-2169-9
Chinese J. Polym. Sci. 2018, 36, 1093–1102

In Situ Synchrotron Radiation Techniques: Watching Deformation-induced Structural Evolutions of Polymers

Liang-Bin Li*

National Synchrotron Radiation Lab, Chinese Academy of Sciences Key Laboratory of Soft Matter Chemistry, Anhui Provincial Engineering Laboratory of Advanced Functional Polymer Film, University of Science and Technology of China, Hefei 230026, China

Abstract Synchrotron radiation (SR) provides highly brilliant light with tunable wavelength from hard X-ray to far infrared, on which scattering, spectroscopy and imaging techniques with high time and spatial resolutions have been developed for *in situ* study on biological system and materials like polymer. With examples on flow-induced crystallization of polymer, deformation of nanoparticle filler network in rubber composite and necking propagation in tensile stretch, current work attempts to demonstrate the advantages of *in situ* synchrotron radiation X-ray scattering, X-ray nano-CT and infrared imaging in the study of deformation-induced multi-scale structural evolutions of polymers. With time resolution up to sub-ms, synchrotron radiation is expected to play a great role in understanding non-equilibrium polymer physics under processing and service conditions, while high-throughput characterization platform based on synchrotron radiation opens the possibility to establish polymer Materials Genome database in processing parameter space within reasonable time, which can serve as the roadmap for industrial polymer processing and accelerate material innovation.

Keywords Synchrotron radiation techniques; X-ray nano-CT; Flow-induced crystallization; Necking propagation; Rubber nanocomposite

Citation: Li, L. B. *In Situ* Synchrotron Radiation Techniques: Watching Deformation-induced Structural Evolutions of Polymers. Chinese J. Polym. Sci. 2018, 36(10), 1093–1102.

INTRODUCTION

Polymer materials consist of hierarchical structures from molecular scale to micrometers. Semicrystalline polymers, occupying about two-thirds of industrial polymer materials, are built with multi-scale structures like crystal lattice, lamellar crystal, spherulite, *etc*., while mixing different polymers or adding inorganic filler in polymers brings extra complexity on structural hierarchy. Under processing and service conditions, polymer materials are generally subjected to large deformation, during which these multi-scale structures undergo fast transformations[1]. Understanding the mechanisms of deformation-induced structural transformations is of importance for guiding industrial processing and predicting service behavior of polymer materials.

To watch deformation-induced structural transformation, *in situ* techniques based on synchrotron radiation are highly desirable. The third generation synchrotron radiation like Shanghai Synchrotron Radiation Facility (SSRF) can provide hard X-ray with about 12 orders higher brilliance than normal laboratory source, which already achieves X-ray scattering measurements with time resolution up to sub-ms or spatial resolution of about 100 nm. These advanced synchrotron radiation techniques provide a great opportunity to study the dynamic structural evolutions under processing and service conditions of polymer materials[2–5].

To demonstrate the advantage of synchrotron radiation, we present several representative examples on the study of deformation-induced structural evolutions of polymers with synchrotron radiation techniques. The time and spatial resolution of X-ray scattering, carried out in SSRF, is illustrated on the study of flow-induced crystallization (FIC) of polymer, while X-ray nano-CT, conducted in Beijing Synchrotron Radiation Facility (BSRF), is employed to unveil nano-filler network in rubber. Micro-infrared imaging performed in National Synchrotron Radiation Lab (NSRL, Hefei) is demonstrated on the study of necking propagation of isotactic polypropylene during tensile deformation.

SYNCHROTRON RADIATION X-RAY SCATTERING (SR-XS)

X-ray scattering and diffraction have been extensively utilized as valuable techniques to characterize the hierarchical structures of polymers from crystal form to lamellar crystals[6, 7]. Combining wide, small and ultra-small angle X-ray scattering techniques (WAXS, SAXS, USAXS), it is possible to follow structures with length scale from sub-nanometer to micrometer, which covers almost the structural hierarchy of polymer materials[8–17].

* Corresponding author: E-mail lbli@ustc.edu.cn

Received April 24, 2018; Accepted June 12, 2018; Published online July 11, 2018

© Chinese Chemical Society
Institute of Chemistry, Chinese Academy of Sciences
Springer-Verlag GmbH Germany, part of Springer Nature 2018

Time Resolved Measurements

FIC is an industrial relevant non-equilibrium phase transition, which is a fast structural evolution driven by external field[18, 19]. Before about 2010, due to the delayed development of detector technique, SR-XS measurements normally could reach a time resolution in the order of seconds. Restricted by time resolution, study on FIC with SR-XS could only follow structural evolution after flow rather than during flow, as a short-term flow in FIC experiments takes times in the order of seconds or less than 1 s. Fortunately, the emergence of new semi-conductor detector like Pilatus allows time resolution to ms or even sub-ms[20–22]. Fig. 1 shows a representative example on the study of FIC with time resolution in ms. To carry out *in situ* measurement, the group in Hefei developed a series of extensional rheometers, which can be installed on SR-XS stations[23–25]. Fig. 1(a) shows the schematic picture of the extensional rheometer, where extension of sample is driven by two rotational drums and a constant strain rate is achieved under a constant motor rotational speed[26]. Combining the extensional rheometer and *in situ* SR-XS measurements, FIC of isotactic polypropylene (*i*PP), polyethylene (PE) and isotactic poly(butane-1) (*i*PB-1) has been systematically studied during and after flow. Figs. 1(b)−1(d) present the engineering stress as a function of time and the corresponding 2D SAXS and WAXS images during extension flow of *i*PP at crystallization temperature T_c of 140 °C, respectively. At a flow time of 234 ms, a stress upturn known as strain hardening occurs, which is accompanied with the occurrence of the streak signal in SAXS (starting at image No. 5 in Fig. 1c) and concomitant highly orientated diffraction of monoclinic α-form crystals in WAXS (Fig. 1d). But the synchronous appearance of SAXS and WAXS signal does not occur at high temperatures. Under the same extensional flow at temperature above 155 °C, SAXS streak signal occurs alone without crystalline diffraction till sample fracture, while from 160 °C to 170 °C no any ordered structural signal is observed in both SAXS and WAXS patterns, but the stress upturn still remains. Inspired by the sequential occurrences of different orderings in temperature space, a tentative kinetic mechanism of nucleation including coil (melt) → stiff segment (helix) → precursor → crystal was proposed. This work demonstrates that the combination of rheological, ultrafast synchrotron radiation SAXS and WAXS measurements is indeed a powerful tool to follow multi-step ordering processes in FIC of polymers.

By tracing the formation condition of crystal structure and morphology in temperature-flow field space, the non-equilibrium phase diagrams of FIC of PE[27], *i*PP[28] and *i*PB-1[21] have been constructed, as shown in Fig. 2, which not only demonstrate the multi-step ordering process in FIC but also highlight the relative stabilities of different phases in temperature-flow field space. Some structures like shish and hexagonal crystal of PE are thermodynamically stable in their phase zones, while structures like β crystal of *i*PP and form III of PB-1 are metastable although they appear during flow. Actually form III of PB-1 has a rather short life time in

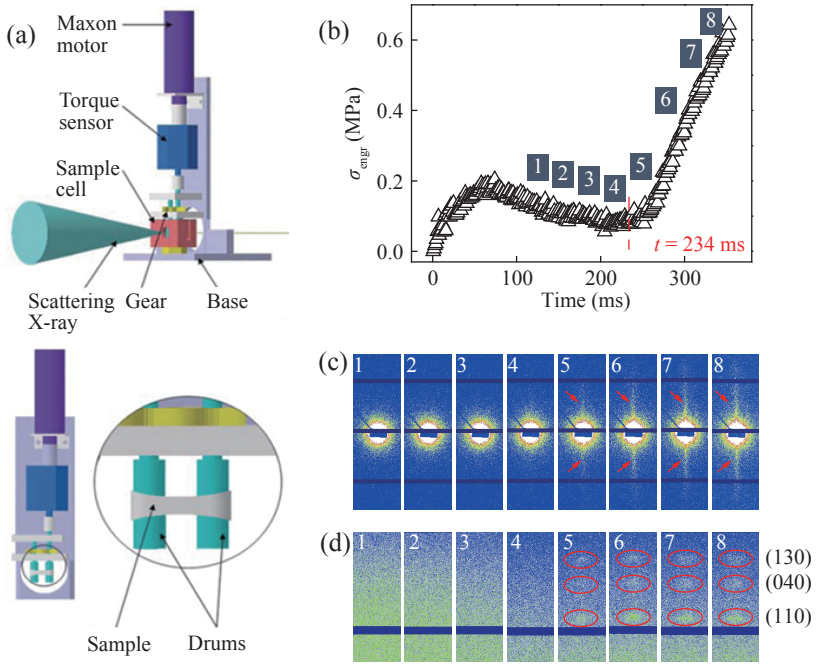


Fig. 1 (a) Schematic drawing of the extensional rheometer for *in situ* SR X-ray scattering measurement; (b) Engineering stress (σ_{engr}) and the corresponding 2D (c) SAXS and (d) WAXS images as a function of time during extension at 140 °C. The digitals from 1 to 8 give correspondence between stress and scattering images. The dashed line, arrows, and ellipses indicate the occurrence of stress-upturn, streak, and crystalline scattering, respectively. The flow direction is horizontal. (Reprinted with permission from Ref. [22]; Copyright (2015) American Chemical Society)

https://doi.org/10.1007/s10118-018-2169-9

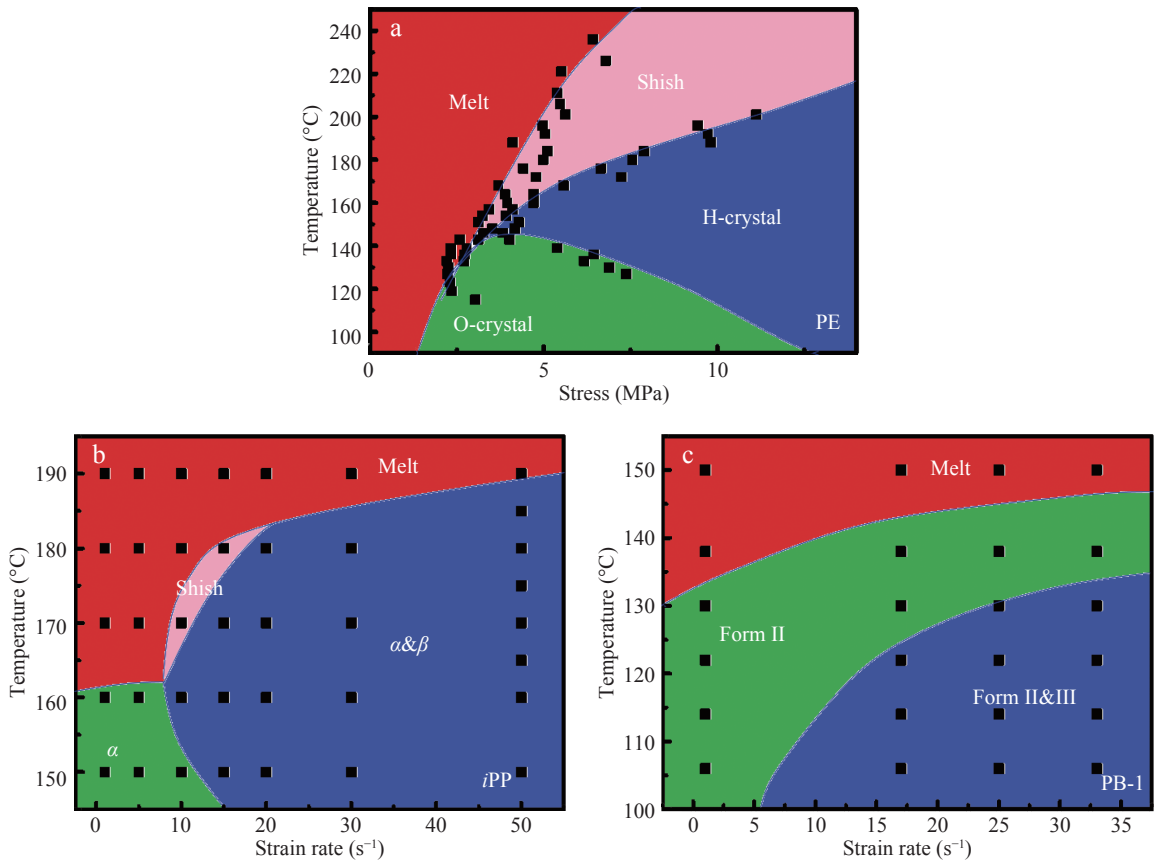


Fig. 2 Non-equilibrium phase diagram of (a) PE, (b) *i*PP and (c) PB-1 in flow-temperature space. M, S, α and β are melt, noncrystalline shish, α crystals and β crystals, respectively (Reprinted with permission from Refs. [27], [28], and [21]; Copyright (2016) Wiley-VCH, Copyright (2017) The Royal Society of Chemistry, and Copyright (2016) Springer Nature)

the orders of tens of ms, which may appear and then disappear during flow. Thus without high time resolved *in situ* SR-XS, it is impossible to observe such a transient metastable phase.

The combination of temperature controlled tensile tester with *in situ* SR-XS has also been widely employed to study the relation of structure-mechanical property. In standard mechanical tensile test on crystallized polymer samples, strain rate is generally at low level, during which a time resolution in tens of seconds can meet the requirement for *in situ* study. However, for post-stretch during the production of high performance fibers and films, strain rate is much faster, which requires high time resolution for *in situ* measurements. Using newly developed SR-XS technique with high time resolution, we have studied the structural evolutions of *i*PP[29–32] and PE[33–36] under different conditions. Fig. 3 presents the summarized results of post-stretch of *i*PP films, which is designed to understand the manufacture of lithium battery separator[37]. Fig. 3(a) demonstrates stress in temperature-strain space, while Figs. 3(b) and 3(c) show the corresponding crystallinity and crystal orientation obtained by *in situ* synchrotron WAXS measurements. Combining mechanical behavior and structural evolutions, the deformation behaviors can be divided into three different zones at different temperature ranges, where different non-linear deformation mechanisms dominate in different zones.

Figs. 2 and 3 also provide a demonstration on the concept of Materials Genome in processing parameter space like temperature, strain and stress. Although fully correlating structure with mechanical behaviors requires more efforts on data analysis, data accumulation is the first and important step for Materials Genome. To this end, SR-XS is definitely a high-throughput technique to collect processing-structure-property information of polymer materials.

Spatial Resolved Measurement

Benefited from the high brilliance of synchrotron radiation, it is possible to focus X-ray to a small spot down to 100 nm. Synchrotron radiation scanning X-ray microscattering (SR-μSXRS) is one technique taking this advantage, which can scan a large interesting area with relatively short time and detect weak signals[38–42]. Combining a shear setup through glass fiber-pulling and SR-μSXRD, Su *et al*. studied FIC of *i*PP and PE[43, 44]. As shear flow field is generated by fiber-pulling, the scanning area is set around the glass fiber. Fig. 4 shows the study on *i*PP as an example. When flow field is imposed at temperatures higher than the melting temperature (T_m is 165 °C), no WAXD signal of the crystal is observed. However, cooling down to 138 °C for isothermal crystallization leads to the appearance of cylindrical crystallites and enhances crystallization kinetics, supporting the existence of flow-induced precursor. Interestingly, *i*PP melt initially sheared at 175 °C shows an induction period

https://doi.org/10.1007/s10118-018-2169-9

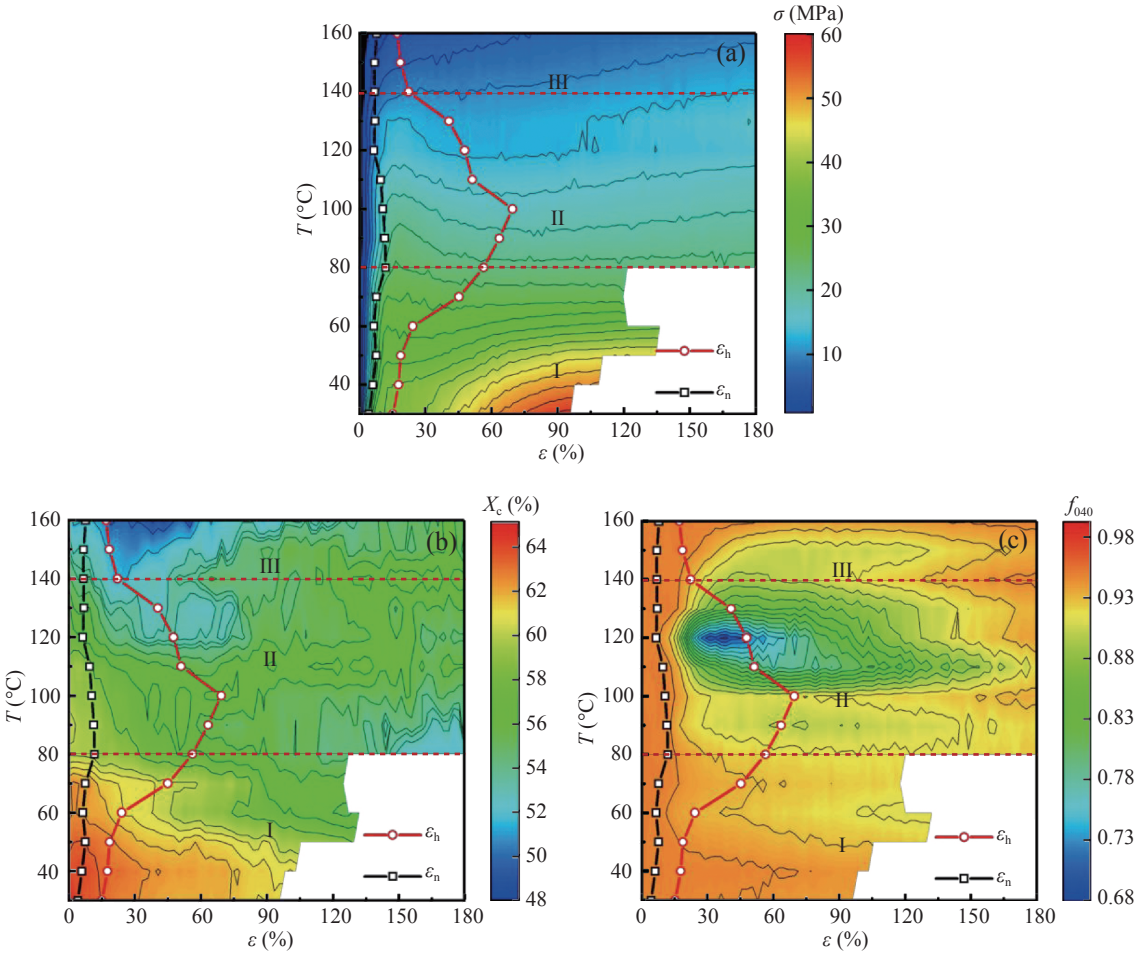


Fig. 3 Contour maps of the evolutions of tensile and structural parameters as a function of strain within experimental temperature range (30–160 °C): (a) engineering stress (σ); (b) crystallinity (X_c); (c) orientation parameter of 040 crystal plane (f_{040}). The black squares are on behalf of ε_n, while the red circles stand for ε_h at different deformation temperatures. (Reprinted with permission from Ref. [32]; Copyright (2018) American Chemical Society)

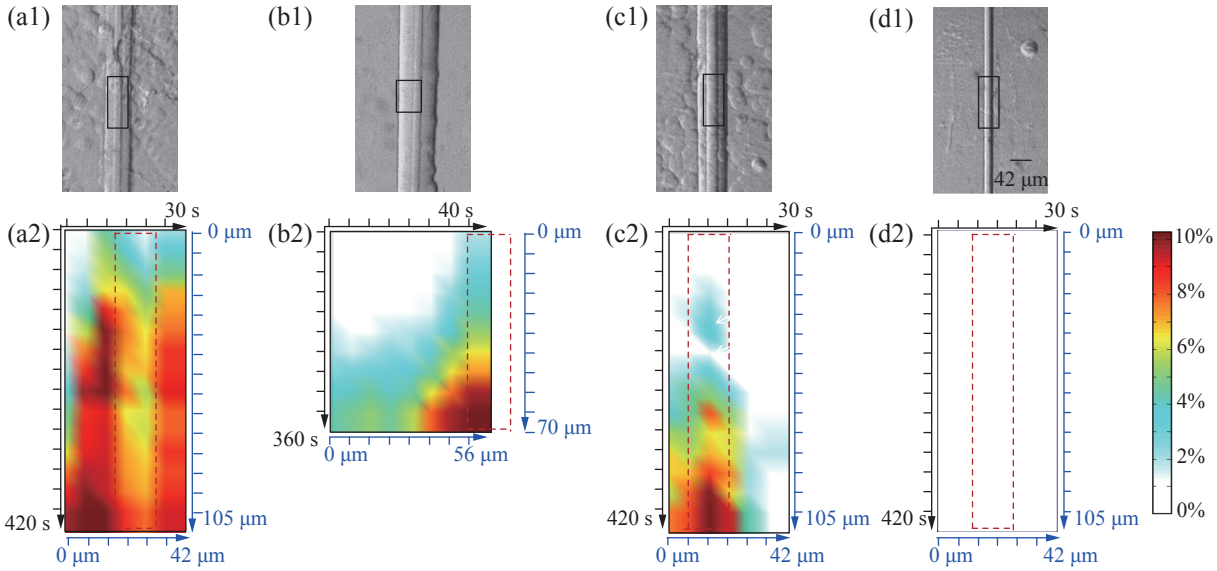


Fig. 4 (a1–d1) Microscopy images after crystallization at 138 °C for about 10 min and (a2–d2) distribution of crystallinity over time around the fiber surface (which is indicated in the microscopy images) during the second SR-μSXRD mapping measurement of samples in (a), (b), (c), and (d) sheared at 160, 170, 175, and 180 °C, respectively and crystallized at 138 °C. The dashed line indicates the position of fiber. (Reprinted with permission from Ref. [43]; Copyright (2014) American Chemical Society)

https://doi.org/10.1007/s10118-018-2169-9

during subsequent crystallization at 138 °C. This clearly demonstrates that the flow-induced orders at 175 °C are non-crystalline precursors. If the flow-induced orders are crystal nucleus, one would observe a direct growth process without induction time.

SR-μSXRS is a powerful technique to detect local structure in heterogeneous samples. We have employed SR-μSXRS to study crystallinity distribution around crack and glass beads in stretched natural rubber[41]. Interestingly, the crystallinity around crack exhibits regions with low and high crystallinities, which construct a soft-hard double network structure and greatly enhance the toughness of natural rubber. Without high spatial resolved SR-μSXRS, the crystallinity around crack would be averaged out and it is impossible to observe the spatial modulation of crystallinity.

SYNCHROTRON RADIATION X-RAY NANO-CT

Filling polymer with nanoparticles is a standard practice in industry. To this respect, rubber/filler composites are one of the best examples. Without filler, most rubbers have too low modulus or toughness, which are somehow useless. However, although reinforcing rubber with nanofillers like carbon black and silica has been carried out for about one century, the underlying mechanism is still under debating. One challenge is related to the hierarchical structure of nanofiller in the matrix rubber. The primary filler particles have diameter in tens of nanometer, which however aggregate into large structure. It has been a long standing hypothesis that filler nanoparticles organize into a network structure in the rubber matrix. Due to its particular length scale, optical and electronic imaging techniques cannot access and view the 3D structure[45–48].

Synchrotron radiation X-ray nano-CT (SR-X nano-CT) has the advantages of high spatial resolution, large view field and high penetration length. In BSRF, SR-X nano-CT is capable of detecting a view field of 60 μm × 60 μm with spatial resolution of 100 nm. A spatial resolution to 30 nm can be achieved with reduced view field of 10 μm × 10 μm, which is still much larger than that of 3D transmission electron microscopy. Fig. 5 shows how the 3D filler network structure is constructed. With SR-X nano-CT measurements, we obtain the aggregates of filler nanoparticles (see Fig. 5a). Then through image analysis, the skeleton of filler aggregates is extracted out as shown in Fig. 5(b). Other structural parameters of filler network, like connectivity and mesh size can also be calculated with image analysis, which can be employed to correlate with mechanical behavior and aid to understand the reinforcement mechanism.

Fig. 6 shows the silica filler networks in silicone rubber at different strains. Imposing strain leads to obvious change of network structure[48]. At strain of 3 and 4, the initial homogeneously distributed network transforms into fibrillar network rich and poor regions, which resembles the picture of phase separation. Interestingly the calculated network connectivity changes weakly even at large strain, indicating simultaneous destruction and reconstruction of network occurs during tensile stretch of silicone rubber composite. In other words, the silica filler network is actually constructed with dynamic reversible bonds, which can break and reform under loading. The dynamic reversible bonds can explain the nearly 1000-time reinforcement effect of silica filler on

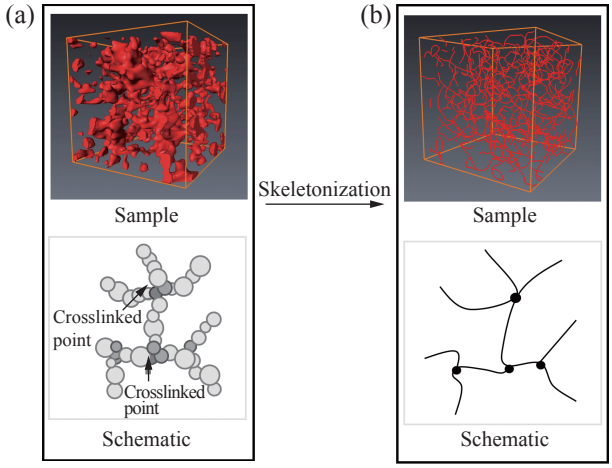


Fig. 5 (a) 3D image of the aggregates of filler nanoparticles obtained from SR-X nano-CT measurements; (b) the extracted skeleton of filler aggregates

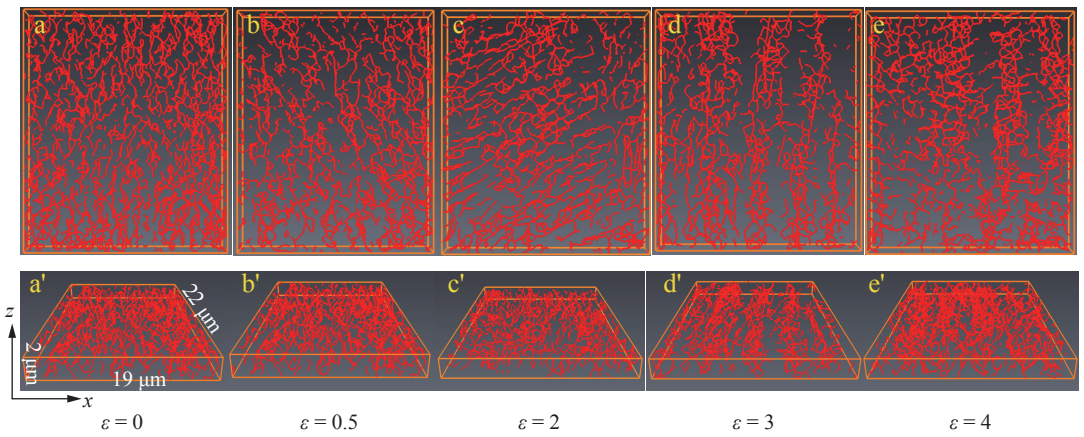


Fig. 6 Constructed filler networks along the backbone of silica aggregates at different strains, which correspond to the thickness of 2 μm (30 pixels) of samples: (a–e) Views of the *x*-*z* plane and (a'–e') tilting 45° to the *x*-*z* plane. The tensile axis is in the *z* direction. (Reprinted with permission from Ref. [48]; Copyright (2017) American Chemical Society)

https://doi.org/10.1007/s10118-018-2169-9

silicone rubber. Indeed under similar loading condition, the network connectivity of carbon black filler in natural rubber is greatly reduced (from about 90% to 40%), indicating carbon black network is not bonded with dynamic reversible interactions. Without dynamic reversible bonds, the reinforcement of carbon black filler on natural rubber is normally in the order of tens, which is one or two orders less than that in silica/silicone rubber system.

The advantage of SR-X nano-CT is the combination of large view field and high spatial resolution as well as large space of sample stage. With a sample size of microns, it gives sufficient statistics to correlate mechanical behavior with structures in 100 nm scale. We envision that further development by combining SR-X nano-CT with nanomechanic tester may provide a great opportunity for the study on structure-mechanics relation of nanomaterial or composites.

SYNCHROTRON RADIATION FOURIER TRANSFORM INFRARED IMAGING (SR-FTIRI)

In addition to high brilliance, synchrotron radiation also provides light with a wide range of tunable wavelength from hard X-ray to far infrared. Compared with normal laboratory infrared source, synchrotron radiation infrared has about two-order higher brilliance, which is well suitable for imaging study[49]. FTIR is one of the most useful techniques in polymer study, which can not only detect chemical species but also differentiate ordered structure and chain orientation[50–54]. With *in situ* SR-FTIRI, it is possible to follow structural distributions such as crystallinity and orientation during deformation[40, 55–57].

Figs. 7 and 8 show an example on the study of necking propagation of *i*PP film during tensile deformation with *in situ* SR-FTIRI[58]. After the occurrence of necking in tensile deformation, three regions exist, namely necking region (NR), transition front (TF) and non-necking region (NNR) in the deformed sample. With SR-FTIRI, it is possible to collect the structure information in these three regions. The absorption spectra with a spatial resolution of 3.9 μm × 3.9 μm can be obtained. Fig. 7(a) presents an optical microscopy image of the deformed sample, while the corresponding spectra at points I (NNR region) and II (NR region) are shown in Fig. 7(b). The solid and dashed curves are spectra with radiation polarized parallel and perpendicular to tensile direction, respectively, which allow us to calculate orientation parameters of amorphous and crystals. With the integrated absorption intensity polarized parallel $A_{\parallel}$ and perpendicular $A_{\perp}$ to the tensile direction, we can calculate dichroic ratio $R = A_{\parallel}/A_{\perp}$. And then orientation parameter can be obtained with $f = \frac{(R-1)}{(R+2)}$. Note that compared with X-ray scattering, FTIR is more effective to measure the orientation of amorphous chain of polymer. Taking absorption intensities of crystal and amorphous bands it is possible to estimate the relative crystallinity X_{cry}. For *i*PP we take 998 and 1153 cm^{-1} bands to represent crystal and amorphous, respectively, and X_{cry} can be expressed as $X_{cry} = \frac{A_{998}}{A_{998} + kA_{1153}}$, where A_{998} and A_{1153} are the absorbance of 998 and 1153 cm^{-1} bands; k (k = 2.75) is the correction factor.

With the spectra obtained from the deformation zone, we can calculate the spatial distributions of crystallinity X_{cry} and the orientation of amorphous chains f. Fig. 8(a) presents the X_{cry} distribution in the deformation zone, which shows a low valley in the transition front (TF). By averaging over X_{cry} through the sample width, we obtained the X_{cry} along tensile axis, which is presented in Fig. 8(b). The low valley at FT is more clearly highlighted while NNR and NR have nearly the same crystallinity. This provides a direct evidence for stretch-induced melting-recrystallization in necking propagation. The melting-recrystallization mechanism is further supported by orientation distribution of amorphous chains. Figs. 8(c) and 8(d) present the 3D and the averaged 1D distributions of amorphous orientation parameter f, respectively. In NNR, amorphous orientation keeps at a low level, while a sharp increase occurs in TF, which is naturally attributed stretch-induced chain orientation. Interestingly,

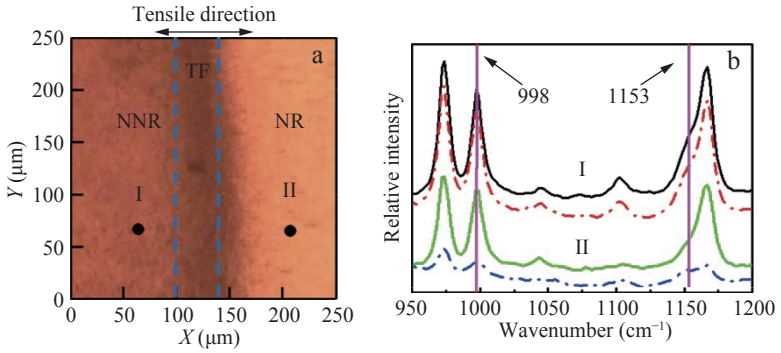


Fig. 7 (a) The optical micrograph at the macroscopic strain of 3.3 of *i*PP film. NNR, TF and NR are defined by the blue dash dot lines. (b) Corresponding FTIR spectra of points I and II in range of 950−1200 cm^{-1}. The solid and dashed lines are spectra with radiation polarized parallel and perpendicular to tensile axis, respectively. (For interpretation of the references to color in this figure legend, readers can refer to the web version of this article) (Reprinted with permission from Ref. [58]; Copyright (2014) Elsevier)

https://doi.org/10.1007/s10118-018-2169-9

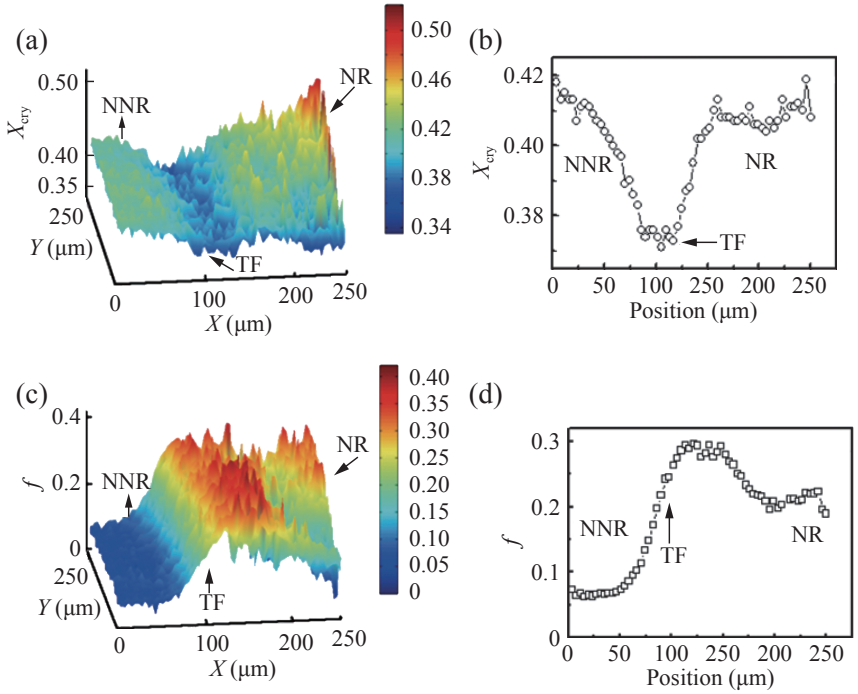


Fig. 8 (a) 3D images of the distribution of X_{cry} and (b) the average X_{cry} along the tensile direction. (c) 3D images of the distribution of orientation parameter f and (d) the average f along the tensile direction. Tensile direction is along X axis. (Reprinted with permission from Ref. [58]; Copyright (2014) Elsevier)

after reaching a maximum amorphous orientation drops down in NR. This phenomenon coincides nicely with the recrystallization process as recrystallization transforms the highly oriented amorphous chains into crystal and consequently reduces the averaged orientation of amorphous chains.

The example shown in Figs. 7 and 8 demonstrates the advantage of *in situ* SR-FTIRI on the study of structural evolutions of polymer, which not only provides spatial resolution but also collects structural information from both amorphous and crystal. Without spatial resolution, the crystallinity would be averaged over all regions. As the TF is quite narrow, such averaging may completely smear out the low valley of crystallinity in TF and cannot show the decrease-increase evolution of crystallinity or melting-recrystallization. Though it is indirect, the non-monotonic evolution of amorphous orientation is also an important evidence to support the mechanism of melting-recrystallization in necking propagation.

In situ SR-FTIRI has also been demonstrated to be an effective tool to study deformation of single fiber like silk, growth front of spherulite and blends[59–63]. Combining spatial resolution and the sensitivity on chemical species and physical structures, SR-FTIRI is expected to play an important role in polymer science, especially on composite materials with structural features in micrometer scale.

CONCLUSIONS AND OUTLOOK

Due to the restriction of the author's knowledge and the article length, current feature article presents only several representative works to demonstrate the advantages of synchrotron radiation X-ray scattering, X-ray Nano-CT and infrared imaging, which allow us to characterize deformation-induced structural transformations of polymers with high time and spatial resolutions. Starting with the successful operation of SSRF in 2009, China has entered a booming era on the development of synchrotron radiation facility. The second phase construction of SSRF has been carried out and Beijing starts to build a new high energy synchrotron radiation facility in 2018. Currently several local governments, including Guangdong, Hubei, Anhui and Sichuan, also invest large budget to support pre-research on new synchrotron facilities. The fast development of synchrotron radiation facilities brings a great opportunity for Chinese polymer community. Here we list four directions in which polymer community may benefit from synchrotron radiation facility.

Non-equilibrium Physics in the Processing and Service Process of Polymer Materials

In polymer processing such as injection molding, film stretch and fiber spinning, polymer melts and/or solutions are subjected to fast and strong deformation, during which the multi-scale structures of polymers undergo a fast evolution process. Similar fast structural evolution also occurs in the service process of polymer materials. For example, in the take-off and landing processes the tires of air plane, mainly built by carbon black filled natural rubber, undergo fast deformation with strain up to 30% and strain rate to 150 s^{-1}. The structural evolutions in the processing and service of polymer are typical non-equilibrium processes mainly driven by external loading. We expect the time resolution of the new

https://doi.org/10.1007/s10118-018-2169-9

USAXS beamline of SSRF and the planed SR-XS beamline with pink X-ray will reach to microsecond, which is sufficient to follow structural evolutions in most processing and service conditions.

Spatial Resolution Required Characterization or Low Scattering System

The high brilliance of synchrotron radiation allows us to characterize low scattering samples like dilute solution, which can largely improve the detection sensitivity. It is also possible to focus beam spot down to nanometer but still keep sufficient flux to collect structural information. Currently the spot size of SR X-ray is already down to 100 nm and we expect a further reduction to 10 nm scale will be achieved in coming years. Thus structural heterogeneity in nanometer scale can be mapped with scanning X-ray scattering, absorption or emission techniques, which may greatly benefit the area of polymer nanomaterials.

Materials Genome in Processing Parameter Space

Material Genome is suggested to be the fourth paradigm for material science and technology, which may largely promote research in material science and accelerate innovation. Currently most efforts in Materials Genome is restricted in composition space rather than processing space. The final properties of polymer productions are not only dependent on their molecular structures and compositions, but also strongly affected by processing-controlled condensed structure and morphology. Materials Genome in processing parameter space, such as temperature, shear or extension rate, strain and pressure, is expected to level up the competence of polymer processing industry. The high time resolution of synchrotron radiation techniques allows us to develop high-throughput research platform, which can efficiently acquire the database for Materials Genome in the processing parameter space. The non-equilibrium phase diagrams shown in Figs. 2 and 3 give a primary example, which may service as the roadmap for polymer processing.

New Techniques Based on Synchrotron Radiation

As synchrotron radiation provides highly brilliant light with wide wavelength range, other advanced techniques, such as resonance scattering and absorption spectroscopy based on soft X-ray[64], single photon ionization with vacuum ultraviolet[65], are also useful tools for polymer science. High energy X-ray is able to get scattering from hydrogen atom, which is an essential element in polymer. Light from synchrotron radiation is polarized, but this property has not been fully explored in the study of polymer materials yet. The development on coherent synchrotron radiation light or free electron laser is expected to bring great opportunities to study polymer dynamics. Similar with dynamic light scattering in visible wavelength range, X-ray photo correlation spectroscopy (XPCS) is a powerful tool to study the dynamics of structures in nanometer and atomic scales[66].

ACKNOWLEDGMENTS

The author would like to thank Dr. Fengmei Su for editing the figures and references, and the former and current members of Soft Matter group in USTC for their contributions on synchrotron experiments. Synchrotron radiation X-ray scattering, Nano-CT and infrared imaging experiments are carried out in SSRF, BSRF and NSRL, respectively. This work was financially supported by the National Natural Science Foundation of China (No. 51633009).

REFERENCES

1 Cui, K.; Ma, Z.; Tian, N.; Su, F.; Liu, D.; Li, L. Multiscale and multistep ordering of flow-induced nucleation of polymers. Chem. Rev. 2018, 118(4), 1840−1886.
2 Tang, Y. J.; Jiang, Z. Y.; Enderle, H. F.; Lilge, D.; Roth, S. V.; Gehrke, R.; Rieger, J.; An, L. J.; Men, Y. F. Mapping the damaged zone around the crack tip in high density polyethylene with synchrotron microfocus small angle X-ray scattering technique. Chinese J. Polym. Sci. 2010, 28(2), 165−170.
3 Lu, Y.; Sun, Y. Y.; Chen, R.; Li, X. H.; Men, Y. F. Deformation temperature and lamellar thickness dependency of Form I to Form III phase transition in syndiotactic polypropylene during tensile stretching. Chinese J. Polym. Sci. 2014, 32(9), 1210−1217.
4 Xu, J. Z.; Chen, C.; Wang, Y.; Tang, H.; Li, Z. M.; Hsiao, B. S. Graphene nanosheets and shear flow induced crystallization in isotactic polypropylene nanocomposites. Macromolecules 2011, 44(8), 2808−2818.
5 Portale, G.; Hermida-Merino, D.; Bras, W. Polymer research and synchrotron radiation perspectives. Eur. Polym. J. 2016, 81, 415−432.
6 Thurman, D. W.; Fernandez-Ballester, L.; Oberhauser, J. P.; Kornfield, J. A. Shear-mediated crystallization of isotactic polypropylene: A wide angle X-ray study of the role of long chains. Abstracts of Papers of the American Chemical Society 2004, 228, U442.
7 Kumaraswamy, G.; Verma, R. K.; Kornfield, J. A.; Yeh, F.; Hsiao, B. S. Shear-enhanced crystallization in isotactic polypropylene. *In situ* synchrotron SAXS and WAXD. Macromolecules 2004, 37(24), 9005−9017.
8 Wang, Z.; Hsiao, B. S.; Sirota, E. B.; Agarwal, P.; Srinivas, S. Probing the early stages of melt crystallization in polypropylene by simultaneous small- and wide- angle X-ray scattering and laser light scattering. Macromolecules 2000, 33(3), 978−989.
9 Ma, Z.; Balzano, L.; Peters, G. W. Dissolution and re-emergence of flow-induced shish in polyethylene with a broad molecular weight distribution. Macromolecules 2016, 49(7), 2724−2730.
10 Ma, Z.; Fernandez-Ballester, L.; Cavallo, D.; Gough, T.; Peters, G. W. M. High-stress shear-induced crystallization in isotactic polypropylene and propylene/ethylene random copolymers. Macromolecules 2013, 46(7), 2671−2680.
11 Cui, K.; Meng, L.; Ji, Y.; Li, J.; Zhu, S.; Li, X.; Tian, N.; Liu, D.; Li, L. Extension-induced crystallization of poly(ethylene oxide) bidisperse blends: an entanglement network perspective. Macromolecules 2014, 47(2), 677−686.
12 Liu, D.; Tian, N.; Cui, K.; Zhou, W.; Li, X.; Li, L. Correlation between flow-induced nucleation morphologies and strain in polyethylene: from uncorrelated oriented point-nuclei, scaffold-network, and microshish to shish. Macromolecules 2013, 46(9), 3435−3443.
13 Liu, Y.; Cui, K.; Tian, N.; Zhou, W.; Meng, L.; Li, L.; Ma, Z.; Wang, X. Stretch-induced crystal-crystal transition of polybutene-1: an *in situ* synchrotron radiation wide-angle X-ray scattering study. Macromolecules 2012, 45(6), 2764−2772.
14 Cui, K. P.; Meng, L. P.; Tian, N.; Zhou, W. Q.; Liu, Y. P.; Wang, Z.; He, J.; Li, L. B. Self-acceleration of nucleation and

formation of shish in extension-induced crystallization with strain beyond fracture. Macromolecules 2012, 45(13), 5477−5486.
15 Matsuba, G.; Zhao, Y. F.; Teratani, M.; Hayashi, Y.; Takayama, Y.; Ogino, Y.; Nishida, K.; Kanaya, T. Oriented structure in isotactic polystyrene melt induced by shear flow. Kobunshi Ronbunshu 2009, 66(10), 419−427.
16 Yan, S.; Wu, Z.; Yu, H.; Gong, Y.; Tan, Y.; Du, R.; Chen, W.; Xing, X.; Mo, G.; Chen, Z. Time-resolved small-angle X-ray scattering study on the growth behavior of silver nanoparticles. J. Phys. Chem. C 2014, 118(21), 11454−11463.
17 Meng, L. P.; Chen, X. W.; Lin, Y. F.; Li, L. B. Improving the softness of BOPP films: from laboratory investigation to industrial processing. Chinese J. Polym. Sci. 2017, 35(9), 1122−1131.
18 Wang, Z.; Ma, Z.; Li, L. Flow-induced crystallization of polymers: molecular and thermodynamic considerations. Macromolecules 2016, 49(5), 1505−1517.
19 Ma, Z.; Balzano, L.; Erp, T. V.; Portale, G.; Peters, G. W. M. Short-term flow induced crystallization in isotactic polypropylene: how short is short? Macromolecules 2013, 46(23), 9249−9258.
20 Li, Z.; Wu, Z.; Mo, G.; Xing, X.; Liu, P. A small-angle X-ray scattering station at Beijing synchrotron radiation facility. Instrum. Sci. Technol. 2014, 42(2), 128−141.
21 Wang, Z.; Ju, J.; Meng, L.; Tian, N.; Chang, J.; Yang, H.; Ji, Y.; Su, F.; Li, L. Structural and morphological transitions in extension-induced crystallization of poly(1-butene) melt. Soft Matter 2017, 13(19), 3639−3648.
22 Cui, K.; Liu, D.; Ji, Y.; Huang, N.; Ma, Z.; Wang, Z.; Lv, F.; Yang, H.; Li, L. Nonequilibrium nature of flow-induced nucleation in isotactic polypropylene. Macromolecules 2015, 48(3), 694−699.
23 Liu, Y.; Zhou, W.; Cui, K.; Tian, N.; Wang, X.; Liu, L.; Li, L.; Zhou, Y. Extensional rheometer for *in-situ* X-ray scattering study on flow-induced crystallization of polymer. Rev. Sci. Instrum. 2011, 82(4), 045104.
24 Meng, L.; Li, J.; Cui, K.; Chen, X.; Lin, Y.; Xu, J.; Li, L. A simple constrained uniaxial tensile apparatus for *in-situ* investigation of film stretching processing. Rev. Sci. Instrum. 2013, 84(11), 115104.
25 Zhang, R.; Ji, Y. X.; Zhang, Q. L.; Ju, J. Z.; Sarmad, A.; Li, L. F.; Zhao, H. Y.; Li, L. B. A universal blown film apparatus for *in situ* X-ray measurements. Chinese J. Polym. Sci. 2017, 35(12), 1508−1516.
26 Yan, T.; Zhao, B.; Cong, Y.; Fang, Y.; Cheng, S.; Li, L.; Pan, G.; Wang, Z.; Li, X.; Bian, F. Critical strain for shish-kebab formation. Macromolecules 2009, 43(2), 602−605.
27 Wang, Z. The non-equilibrium phase diagrams of flow-induced crystallization and melting of polyethylene. Sci. Rep. 2016, 6, 32968.
28 Ju, J.; Wang, Z.; Su, F.; Ji, Y.; Yang, H.; Chang, J.; Ali, S.; Li, X.; Li, L. Extensional flow-induced dynamic phase transitions in isotactic polypropylene. Macromol. Rapid Commun. 2016, 37(17), 1441−1445.
29 Chen, X.; Lv, F.; Su, F.; Ji, Y.; Meng, L.; Wan, C.; Lin, Y.; Li, X.; Li, L. Deformation mechanism of *i*PP under uniaxial stretching over a wide temperature range: An *in-situ* synchrotron radiation SAXS/WAXS study. Polymer 2017, 118, 12−21.
30 Chen, L.; Zhou, W.; Su, F.; Zhang, W.; Chen, P.; Ji, Y.; Li, L. Filler-induced heterogeneous distribution of stretch-induced crystallization in natural rubber: An *in-situ* synchrotron-radiation micro-focused scanning X-ray diffraction study. Polymer 2017, 115, 217−223.
31 Lin, Y.; Meng, L.; Wu, L.; Li, X.; Chen, X.; Zhang, Q.; Zhang, R.; Zhang, W.; Li, L. A semi-quantitative deformation model for pore formation in isotactic polypropylene microporous membrane. Polymer 2015, 80, 214−227.
32 Lin, Y.; Li, X.; Meng, L.; Chen, X.; Lv, F.; Zhang, Q.; Zhang, R.; Li, L. Structural evolution of hard-elastic isotactic polypropylene film during uniaxial tensile deformation: the effect of temperature. Macromolecules 2018, 51(7), 2690−2705.
33 Lv, F.; Chen, X.; Wan, C.; Su, F.; Ji, Y.; Lin, Y.; Li, X.; Li, L. Deformation of ultrahigh molecular weight polyethylene precursor fiber: crystal slip with or without melting. Macromolecules 2017, 50(17), 6385−6395.
34 Li, X.; Lin, Y.; Su, F.; Chen, X.; Lv, F.; Meng, L.; Zhang, Q.; Li, L. Stabilization mechanism of micropore in high-density polyethylene: a comparison between thermal and mechanical pathways. Macromol. Mater. Eng. 2017, 302(10), 1700178.
35 Li, X.; Meng, L.; Lin, Y.; Chen, X.; Zhang, Q.; Zhang, R.; Wu, L.; Zhang, W.; Li, L. Preparation of highly oriented polyethylene precursor film with fibril and its influence on microporous membrane formation. Macromol. Chem. Phys. 2016, 217(8), 974−986.
36 Li, X.; Lin, Y.; Ji, Y.; Meng, L.; Zhang, Q.; Zhang, R.; Zhang, W.; Li, L. Strain and temperature dependence of deformation mechanism of lamellar stacks in HDPE and its guidance on microporous membrane preparation. Polymer 2016, 105, 264−275.
37 Lin, Y.; Li, X.; Meng, L.; Chen, X.; Lv, F.; Zhang, Q.; Zhang, R.; Li, L. Structural evolution of hard-elastic isotactic polypropylene film during uniaxial tensile deformation: the effect of temperature. Macromolecules 2018, 51(7), 2690−2705.
38 Kanaya, T.; Polec, I. A.; Fujiwara, T.; Inoue, R.; Nishida, K.; Matsuura, T.; Ogawa, H.; Ohta, N. Precursor of shish-kebab above the melting temperature by microbeam X-ray scattering. Macromolecules 2013, 46(8), 3031−3036.
39 Gutiérrez, M. C. G.; Alfonso, G. C.; Riekel, C.; Azzurri, F. Spatially resolved flow-induced crystallization precursors in isotactic polystyrene by simultaneous small- and wide-angle X-ray microdiffraction. Macromolecules 2004, 37(2), 478−485.
40 Su, F. M.; Li, X. Y.; Zhou, W. M.; Zhu, S. S.; Ji, Y. X.; Wang, Z.; Qi, Z. M.; Li, L. B. Direct formation of isotactic poly(1-butene) form I crystal from memorized ordered melt. Macromolecules 2013, 46(18), 7399−7405.
41 Zhou, W.; Li, X.; Lu, J.; Huang, N.; Chen, L.; Qi, Z.; Li, L.; Liang, H. Toughening mystery of natural rubber deciphered by double network incorporating hierarchical structures. Sci. Rep. 2014, 4, 7502.
42 Melnikov, A.; Rosenthal, M.; Rodygin, A.; Doblas, D.; Anokhin, D.; Burghammer, M.; Ivanov, D. Re-exploring the double-melting behavior of semirigid-chain polymers with an *in-situ* combination of synchrotron nano-focus X-ray scattering and nanocalorimetry. Eur. Polym. J. 2016, 81, 598−606.
43 Su, F.; Zhou, W.; Li, X.; Ji, Y.; Cui, K.; Qi, Z.; Li, L. Flow-induced precursors of isotactic polypropylene: an *in situ* time and space resolved study with synchrotron radiation scanning X-ray microdiffraction. Macromolecules 2014, 47(13), 4408−4416.
44 Su, F.; Ji, Y.; Meng, L.; Chang, J.; Chen, L.; Li, L. Shear-induced precursors in polyethylene: An *in-situ* synchrotron radiation scanning X-ray microdiffraction study. Polymer 2018, 135, 61−68.
45 Chen, L.; Chen, W.; Zhou, W.; Li, J.; Liu, Y.; Qi, Z.; Li, L. *In situ* microscopic infrared imaging study on deformation-induced spatial orientation and phase transition distributions of PA12. J. Appl. Polym. Sci. 2014, 131(17), 40703.
46 Chen, L.; Song, L.; Li, J.; Chen, P.; Huang, N.; Li, L. From the volume-filling effect to the stress-bearing network: the reinforcement mechanisms of carbon black filler in natural rubber. Macromol. Mater. Eng. 2016, 301(11), 1390−1401.
47 Chen, L.; Zhou, W.; Lu, J.; Li, J.; Zhang, W.; Huang, N.; Wu,

L.; Li, L. Unveiling reinforcement and toughening mechanism of filler network in natural rubber with synchrotron radiation X-ray nano-computed tomography. Macromolecules 2015, 48(21), 7923−7928.
48 Song, L.; Wang, Z.; Tang, X.; Chen, L.; Chen, P.; Yuan, Q.; Li, L. Visualizing the toughening mechanism of nanofiller with 3D X-ray nano-CT: stress-induced phase separation of silica nanofiller and silicone polymer double networks. Macromolecules 2017, 50(18), 7249−7257.
49 Ellis, G. J.; Martin, M. C. Opportunities and challenges for polymer science using synchrotron-based infrared spectroscopy. Eur. Polym. J. 2016, 81, 505−531.
50 Geng, Y.; Wang, G.; Cong, Y.; Bai, L.; Li, L.; Yang, C. Shear-induced nucleation and growth of long helices in supercooled isotactic polypropylene. Macromolecules 2009, 42(13), 4751−4757.
51 An, H.; Li, X.; Geng, Y.; Wang, Y.; Wang, X.; Li, L.; Li, Z.; Yang, C. Shear-induced conformational ordering, relaxation, and crystallization of isotactic polypropylene. J. Phys. Chem. B 2008, 112(39), 12256−12262.
52 An, H.; Zhao, B.; Ma, Z.; Shao, C.; Wang, X.; Fang, Y.; Li, L.; Li, Z. Shear-induced conformational ordering in the melt of isotactic polypropylene. Macromolecules 2007, 40(14), 4740−4743.
53 Santoro, G.; Ochando, I. M.; Ellis, G. Advanced vibrational microspectroscopic study of conformational changes within a craze in poly(ethylene terephthalate). Macromolecules 2015, 48(4), 1162−1168.
54 Dumas, P.; Jamin, N.; Teillaud, J.; Miller, L.; Beccard, B. Imaging capabilities of synchrotron infrared microspectroscopy. Faraday Discuss. 2004, 126, 289−302.
55 Li, H.; Zhou, W.; Ji, Y.; Hong, Z.; Miao, B.; Li, X.; Zhang, J.; Qi, Z.; Wang, X.; Li, L.; Li, Z. M. Spatial distribution of crystal orientation in neck propagation: An *in-situ* microscopic infrared imaging study on polyethylene. Polymer 2013, 54(2), 972−979.
56 Su, F. M.; Li, X. Y.; Zhou, W. M.; Chen, W.; Li, H. L.; Cong, Y. H.; Hong, Z. H.; Qi, Z. M.; Li, L. B. Accelerating crystal-crystal transition in poly(1-butene) with two-step crystallization: An *in-situ* microscopic infrared imaging and microbeam X-ray diffraction study. Polymer 2013, 54(13), 3408−3416.
57 Hong, Z.; Cong, Y.; Qi, Z.; Li, H.; Zhou, W.; Chen, W.; Wang, X.; Zhou, Y.; Li, L. Studying deformation behavior of a single spherulite with *in-situ* infrared microspectroscopic imaging. Polymer 2012, 53(2), 640−647.
58 Li, J.; Li, H.; Meng, L.; Li, X.; Chen, L.; Chen, W.; Zhou, W.; Qi, Z.; Li, L. *In-situ* MR imaging on the plastic deformation of *i*PP thin films. Polymer 2014, 55(5), 1103−1107.
59 Cong, Y.; Hong, Z.; Zhou, W.; Chen, W.; Su, F.; Li, H.; Li, X.; Yang, K.; Yu, X.; Qi, Z. Conformational ordering on the growth front of isotactic polypropylene spherulite. Macromolecules 2012, 45(21), 8674−8680.
60 Ling, S.; Qi, Z.; Knight, D. P.; Shao, Z.; Chen, X. Synchrotron FTIR microspectroscopy of single natural silk fibers. Biomacromolecules 2011, 12(9), 3344−3349.
61 Cong, Y. H.; Hong, Z. H.; Qi, Z. M.; Zhou, W. M.; Li, H. L.; Liu, H.; Chen, W.; Wang, X.; Li, L. B. Conformational ordering in growing spherulites of isotactic polypropylene. Macromolecules 2010, 43(23), 9859−9864.
62 Chen, X.; Shao, Z.; Marinkovic, N. S.; Miller, L. M.; Zhou, P.; Chance, M. R. Conformation transition kinetics of regenerated Bombyx mori silk fibroin membrane monitored by time-resolved FTIR spectroscopy. Biophys. Chem. 2001, 89(1), 25−34.
63 Lewis, E. N.; Treado, P. J.; Reeder, R. C.; Story, G. M.; Dowrey, A. E.; Marcott, C.; Levin, I. W. Fourier transform spectroscopic imaging using an infrared focal-plane array detector. Anal. Chem. 1995, 67(19), 3377−3381.
64 Liu, F.; Brady, M. A.; Wang, C. Resonant soft X-ray scattering for polymer materials. Eur. Polym. J. 2016, 81, 555−568.
65 Qi, F. Combustion chemistry probed by synchrotron VUV photoionization mass spectrometry. P. Combust. Inst. 2013, 34(1), 33−63.
66 Sikharulidze, I.; Dolbnya, I. P.; Fera, A.; Madsen, A.; Ostrovskii, B. I.; de Jeu, W. H. Smectic membranes in motion: Approaching the fast limits of X-ray photon correlation spectroscopy. Phys. Rev. Lett. 2002, 88(11), 115503.

https://doi.org/10.1007/s10118-018-2169-9